Graphite-Incorporated MoS_2 Nanotubes: A New Coaxial Binary System

C. Reza-San Germán,[†,‡,§] P. Santiago,[*,‡] J. A. Ascencio,[†,∥] U. Pal,[⊥] M. Pérez-Alvarez,[§] L. Rendón,[‡] and D. Mendoza[#]

Facultad de Química, Universidad Autónoma del Estado de México, Paseo Colon esq. Paseo Tollocan, Apartado Postal A-20, Toluca, C.P. 50120, Instituto de Física, Universidad Nacional Autónoma de México, Apartado Postal 20-364, 01000 México D.F., Instituto Nacional de Investigaciones Nucleares, Km. 36.5, Carretera México-Toluca, Mpio. de Ocoyoacac, Edo. de México, C.P. 52045, Instituto Mexicano del Petróleo, Eje Lázaro Cárdenas 152, Col. San Bartolo Atepehuacan, México D.F., C.P. 07730, Instituto de Física, Universidad Autónoma de Puebla, Apdo. Postal J-48, Puebla, Pue. 72570, and Instituto de Investigaciones en Materiales, Universidad Nacional Autónoma de México, Apartado Postal 70-360, 04510 México D.F., Mexico

Received: April 26, 2005; In Final Form: July 1, 2005

Graphite-filled MoS_2 nanotubes were synthesized by pyrolizing propylene inside MoS_2 nanotubes prepared by a template-assisted technique. The large coaxial nanotubes were constituted of graphite sheets inserted between the MoS_2 layers, forming the outer part, and coaxial multiwall carbon nanotubes intercalated with MoS_2 inside. High-resolution electron microscopy (HREM) and electron energy loss spectroscopy techniques along with molecular dynamics simulation and quantum mechanical calculations were used to characterize the samples. The one-dimensional structures exhibit diverse morphologies such as long straight and twisted nanotubes with several structural irregularities. The interplanar spacing between the MoS_2 layers was found to increase from 6.3 to 7.4 Å due to intercalation with carbon. Simulated HREM images revealed the presence of mechanical strains in the carbon-intercalated MoS_2 layers as the reason for obtaining these twisted nanostructures. The mechanism of formation of carbon-intercalated MoS_2 tubular structures and their stability and electronic properties are discussed. Our results open up the possibility of using MoS_2 nanotubes as templates for the synthesis of new one-dimensional binary-phase systems.

Introduction

Since the discovery of the nanotubes by Iijima,[1] improving the methods for producing both carbon[2,3] and inorganic[4−7] tubular structures has been the goal of many researchers. The perspective of applications of these nanostructures has also determined the imperative necessity of understanding their morphology, composition, and physicochemical properties.[8,9] The synthesis of metal chalcogenide nanotubes has been reported by several authors.[6,7] One of the most controllable and inexpense methods to produce one-dimensional nanostructured materials is the use of templates, such as Al_2O_3 nanoporous molds prepared by an anodization process.[10,11] Utilizing the chemical and thermal stability,[12−14] insulating behavior, and possibility of controlling the diameter of the channels and pore density through controlled anodization,[15] aluminum oxide is traditionally used for preparing amorphous anodic alumina nanoporous templates (AANTs) highly suitable for generating one-dimensional nanostructure systems. The AANTs prepared in this way can further be modified by filling any material in its hollow structure and can be reused as a new cast to combine two or more different materials. Several workers have synthesized MoS_2 nanotubes of controlled length and diameter utilizing AANTs. Generally, these nanotubes are of multiwall or layered structures.

The possibility of having a material with the extraordinary properties of both carbon and MoS_2 nanotubes in a host−guest configuration may open up a new field in the study of novel coaxial heterogeneous structures. Recently, the studies of host−guest intercalation between atomic and molecular species in layered matrixes such as graphite and metal dichalcogenide structures such as QS_2 compounds[16] have been started. Though the intercalation chemistry of transition-metal sulfides has been well-known since the 1970s, molybdenum disulfide nanotube chemistry is relatively recent, and the synthesis of tubular structures of MoS_2 and their physicochemical properties are still under study.[17−19] However, the synthesis of tubular nanostructures of binary phase utilizing the layered morphology of metal chalcogenides is still a challenge.

The design and manipulation of the nanostructured materials involve a complete study of the atomic distribution and its corresponding effects on the electronic structure. Chemical, photonic, and electronic properties of nanostructure materials[20−23] have been determined routinely utilizing their crystallographic structures. Therefore, a combination of methods such as high-resolution electron microscopy and molecular dynamics simulation permit nanostructured materials to be studied with enough detail of their structural and physicochemical characteristics.[24−26]

In the present work, we report on the synthesis and characterization of new MoS_2−C coaxial mixed nanotube structures with several morphologies. The nanostructures were characterized using high-resolution electron microscopy (HREM) and

* To whom correspondence should be addressed. E-mail: paty@fisica.unam.mx.
† Universidad Autónoma del Estado de México.
‡ Instituto de Física, Universidad Nacional Autónoma de México.
§ Instituto Nacional de Investigaciones Nucleares.
∥ Instituto Mexicano del Petróleo.
⊥ Universidad Autónoma de Puebla.
Instituto de Investigaciones en Materiales, Universidad Nacional Autónoma de México.

10.1021/jp052174e CCC: $30.25
Published on Web 08/27/2005

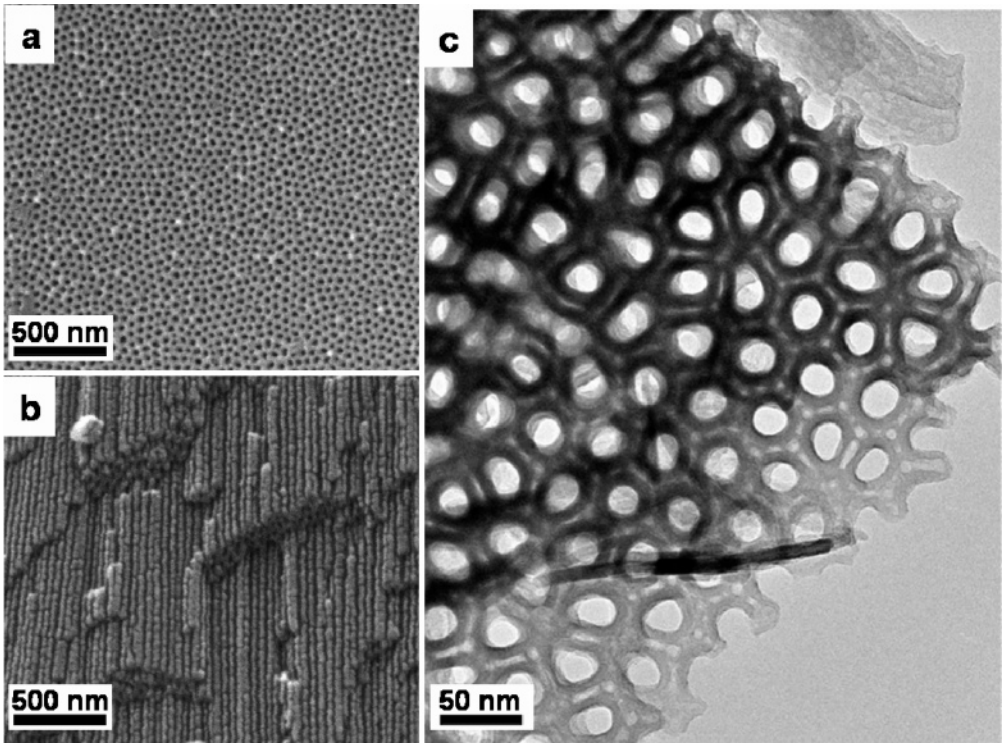

Figure 1. Typical SEM micrographs. (a) Planar and (b) cleaved section of the anodized alumina template used in this study. Formation of hexagonal pores of about 30 nm average diameter and 50 μm average length were observed. (c) TEM micrograph of the AANT cross section.

electron energy loss spectroscopy (EELS) techniques. Molecular dynamics (MD) simulations and quantum mechanics calculations were performed to understand the mechanism of formation of the nanostructures and their stability and electronic properties.

Experimental Procedure

Large coaxial and intercalated nanotubes of MoS_2 and carbon (MoS_2−C) were synthesized through a template growth approach using AANTs. Amorphous AANTs were prepared in an electrolytic cell using two aluminum electropolished sheets as electrodes immersed in an aqueous H_2SO_4 solution (5%) at a controlled dc voltage (5 V). To obtain homogeneous AANTs, the temperature of the electrolytic cell was kept in the range of 0−5 °C and the anodization was carried out for 8 h. The polarity of the electrolytic cell was reverted to separate the AANTs from the aluminum anode. The impervious layer of the film was then removed by immersing it in a 20% sulfuric acid solution for 10 min. Layers of several micrometers thickness with local hexagonal close-packed structure were obtained. The AANTs prepared in this way are thermally and structurally stable up to 900 °C.[12−14] In Figure 1, typical microscopic views of planer and sectional surfaces of the template used in this study are shown.

The first step of generating the MoS_2−C nanotubes was the synthesis of the host structure. MoS_2 nanotubes were obtained by pyrolizing $(NH_4)_2MoS_4$ inside the template using a solution of $(NH_4)_2MoS_4$ (0.1 M) and dimethylformamide (DMF) as the solution-phase precursor.[10] A nanoporous alumina template 1 cm^2 in size and 50 μm in thickness was immersed in the precursor solution for 5 min and then dried at 70 °C to evaporate the remaining solvent at the surface. The precursor was pyrolized at 450 °C for 1 h inside a programmable horizontal furnace under the flow of a hydrogen and nitrogen gas mixture (10% H_2, 20 mL/min). The details of the synthesis technique have already been reported by Zelenski[28] and P. Santiago et al.[10] The special feature of the MoS_2 nanotubes synthesized in the present case is that over 90% of them had a morphology of a chain of interconnected bent segments, while the rest had a long straight tubular structure.

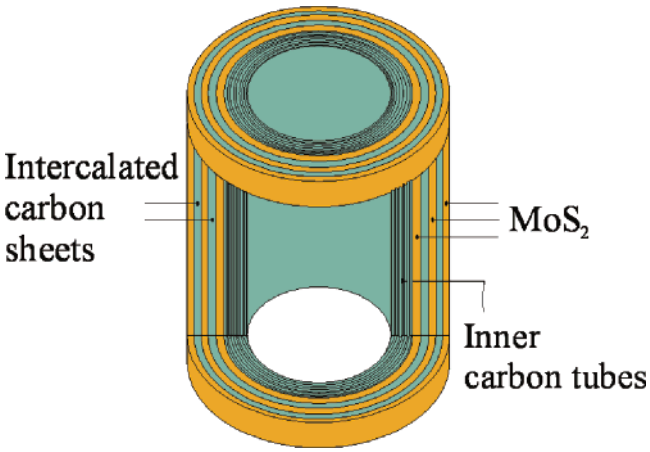

Figure 2. Schematic diagram of a coaxial intercalated MoS_2−C nanotube with a pure graphite phase inside.

Once the AANT was filled with MoS_2 nanotubes, the sample was again loaded into the furnace for the graphitization and intercalation process. A propylene/N_2 mixture flux (1:8 v/v, 2 mL/min) was passed through the furnace at 800 °C for 1 h. To isolate the synthesized nanostructures from the template, it was loaded into an acid digestion bomb filled with 1 M sodium hydroxide solution. The system was heated at 120 °C on a hot plate for 12 h. This alumina-dissolving process generates aluminum oxyhydroxide residues in the form of a gel suspended in the sodium hydroxide solution. The reaction products [$2NaOH + Al_2O_3 \cdot 3H_2O \rightarrow 2NaOH + 2Al(OH)_{3(gel)}$] were carefully removed with a syringe and substituted with distilled water several times to separate the nanotubes from these residues. Finally, distilled water was substituted with methanol, and the resultant solid material was dispersed in an ultrasonic bath for

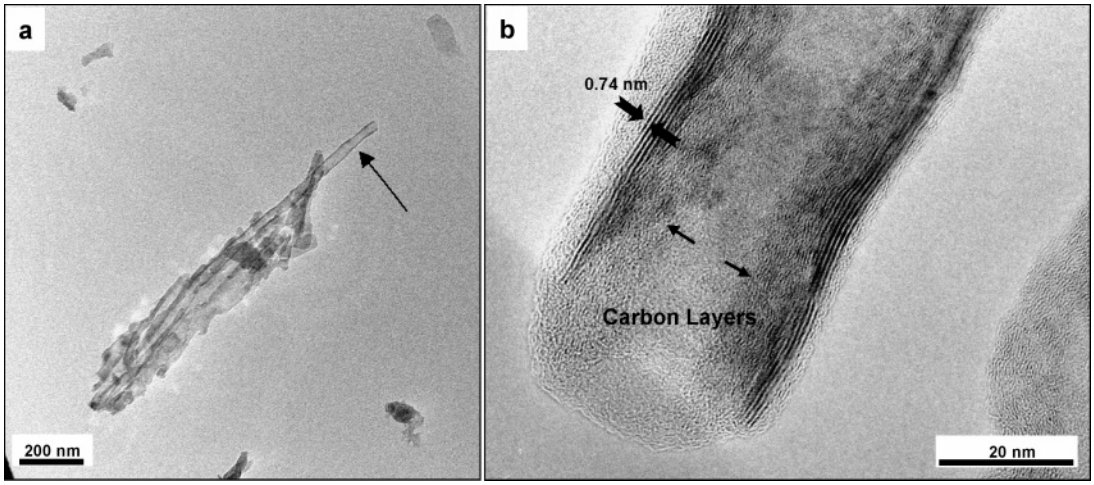

Figure 3. (a) A typical low-magnification TEM micrograph of the binary-phase nanotubes and (b) an HREM micrograph showing their layered structures.

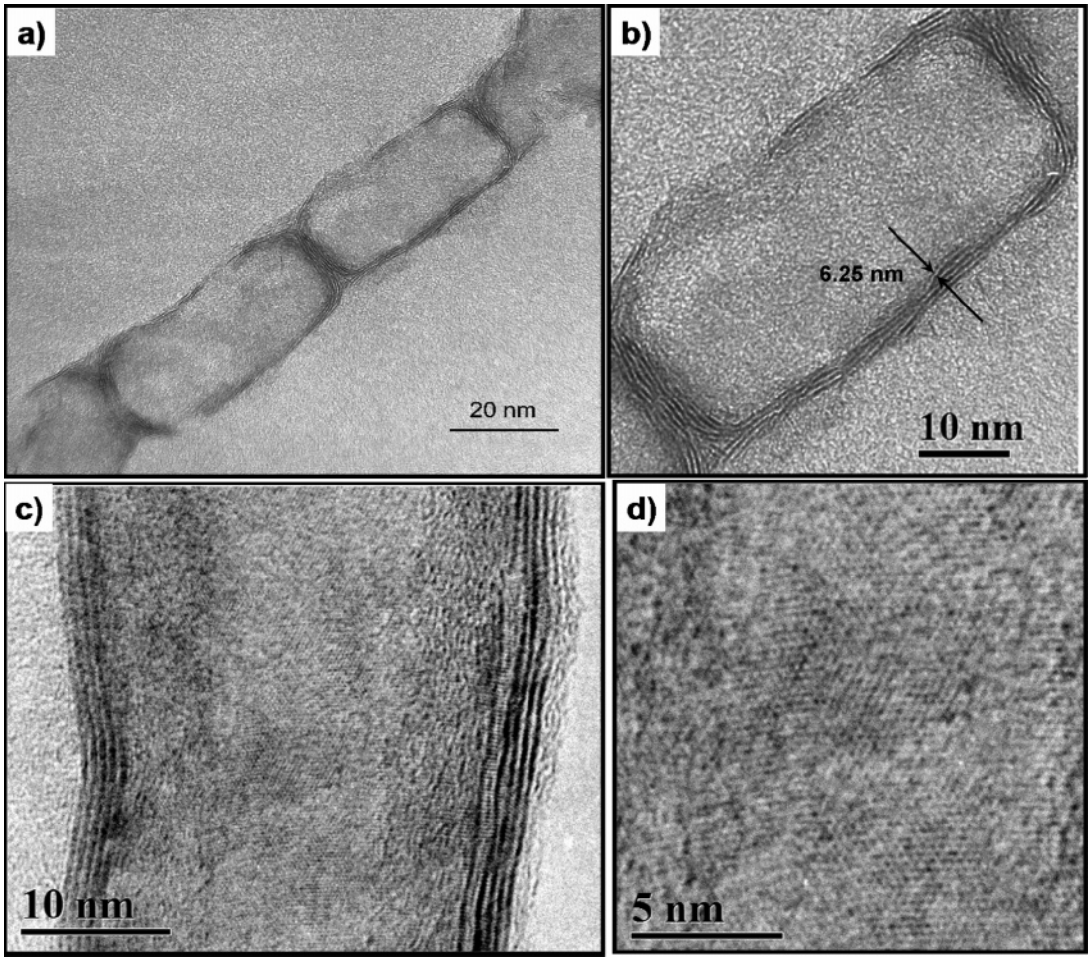

Figure 4. (a, b) Typical HREM micrographs of pure MoS_2 nanotubes. (c) HREM micrograph of MoS_2−C, showing hexagonal Moire fringes at the central part of the nanotubes. (d) A closer view of the selected area marked in (c).

5 min. A drop of the suspension was put on a carbon-coated copper grid for TEM analysis.

TEM observations were performed in a JEM 2010 FasTem analytical microscope equipped with a GIF (Gatan image filter) and *Z*-contrast annular detectors. High-resolution images were obtained at the optimum focus condition (Sherzer condition), and a defocus condition was used to improve the contrast of the nanotube walls. The chemical composition of the nanotubes was analyzed through the GIF detector, acquiring an EELS spectrum in diffraction mode.

Crystal Builder, Force-Field, and HRTEM modules of the Cerius[2] simulation software of Accelrys were used to simulate the crystalline nanotube structures and corresponding HREM images.[24] The crystalline models were generated using the Crystal Builder module based on the MoS_2 and C atomic positions, symmetry conditions, and lattice parameters. The most stables models for MoS_2−C nanotubes were obtained using a force field method.[25,26] The corresponding simulated HREM images for these models were obtained using the SimulaTEM software[29] based on the multislice method.

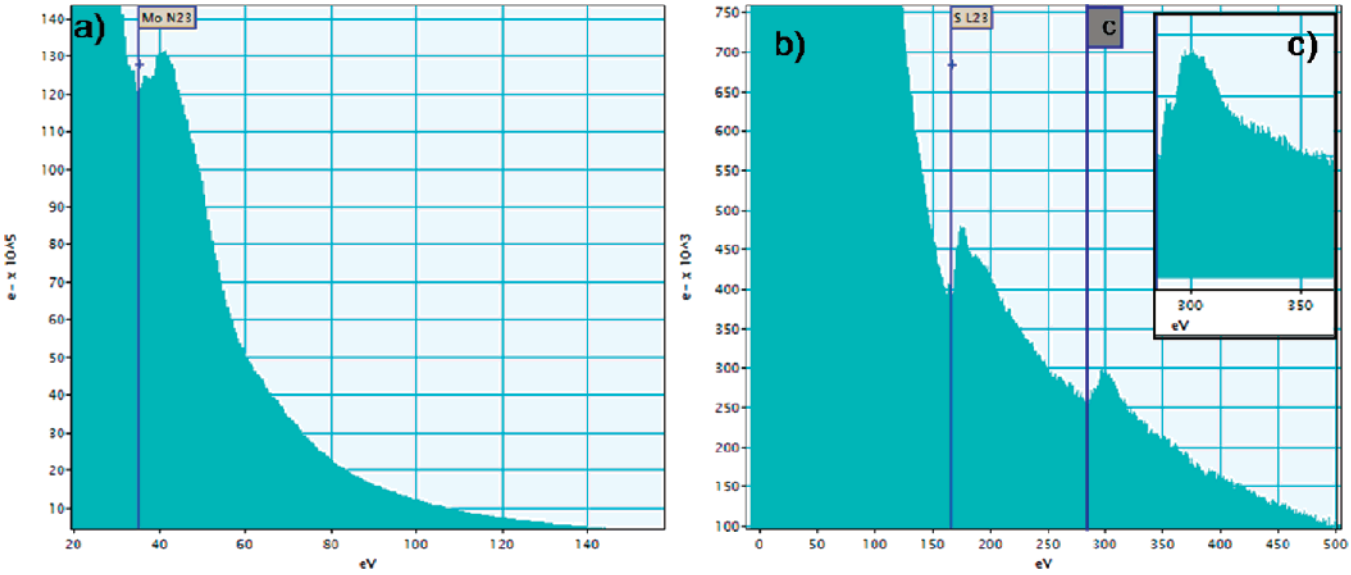

Figure 5. EELS spectrum obtained from a single tube in diffraction mode: (a) magnification of the spectrum at the Mo edge (35 eV), (b) zoomed spectrum at the sulfur and carbon edges (165 and 284 eV, respectively), and (c) magnified part at the carbon zone showing a typical graphite spectrum.

A theoretical analysis of carbon-intercalating effects in the MoS_2 structure was initially made for a periodic structure using the CASTEP software.[30] This module is based on a wave plane method using the gradient-corrected approximation (GCA) and the Perdew−Burke−Ernzerhof functional.[31] To determine the density of states and changes in electrostatic potential in carbon-intercalated MoS_2, a geometry optimization procedure was considered with convergence tolerance steps of 5×10^{-6} eV/atom, a self-consistent field tolerance of 5×10^{-7} eV/atom for each single-point energy calculation, and a $9 \times 9 \times 2$ *k*-point set.

Results and Discussion

Layered compounds such as MoS_2 have a good hosting capacity because of their intercalating spaces.[32] The intercalation process is associated with the weakening of the van der Waals forces between the metal dichalcogenide layers.[33] In the present work, the graphitization process through the pyrolysis of propylene gas generated the intercalation of carbon sheets between the layers of MoS_2 host nanotubes. Through this mechanism, multiwall nanotubes of binary phase containing pieces of carbon layers intercalated between the MoS_2 walls were produced. Additionally, single-phase carbon nanotubes were formed inside the intercalated nanotubes, generating coaxial binary entities. A schematic diagram of this one-dimensional structure is shown in Figure 2.

Figure 3a shows a low-magnification TEM micrograph of the sample, illustrating the presence of several nanotubes of different sizes. The contrast differences at the edges of the tubes are evident in the micrograph. The length of the tubes varied from 500 to 1000 nm with a mean internal diameter of around 30 nm. The tubular structures observed in this particular sample are exceptionally straight compared to the elliptical cage linked chain structures, generally observed in MoS_2 nanotubes produced by the template mechanism.[10] Such a difference in morphology might be due to the difference in the mechanical properties between the nanostructures. In contrast to the binary phase, the pure MoS_2 nanotubes were more flexible (revealing folded structures in SEM micrographs). The HREM contrast observed at the external layers of the tubes (Figure 3b) is very similar to the usual contrast of pure MoS_2 nanotube walls and

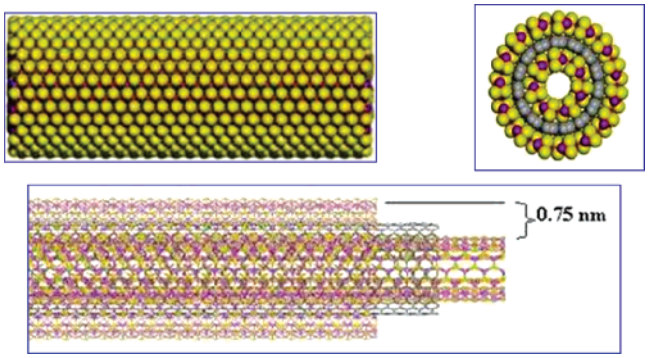

Figure 6. Lateral and sectional views (right corner and bottom) of a stable configuration of intercalated graphite slabs with a stoichiometric MoS_2 nanotube, generated using the molecular dynamics simulation process. The distance between the MoS_2 layers after the energy minimization procedure is 7.5 Å.

alkali-metal-intercalated MoS_2 layers.[33] The average interatomic layer distances were obtained using AnalySIS software from Soft Imaging System,[34] taking measurements at 10 different locations in 10 different tubes. Our estimated average interlayer distance for the external layers was 7.4 ± 0.05 Å in comparison with the 6.25 Å value reported for pure MoS_2 nanotubes.[10] The disordered features surrounding the nanotubes shown in Figure 3a might be the fragments of aluminum hydroxide remaining on them after washing, during the template separation process. In Figure 4, typical HREM images of pure MoS_2 and graphite-incorporated MoS_2 nanotubes are presented. The contrast difference between the two samples is clear from the images. A closer view of the graphite-incorporated MoS_2 nanotubes reveals zones with highly defective graphitic layers at the inner surface of the main tube (Figure 4c). The average interplanar spacing estimated for this region was about 3.5 ± 0.05 Å, which is higher than the interplaner spacing of common (0002) graphite planes. However, such an expansion of interplanar distance has been observed previously in disordered graphite sheets.[36,37]

The hexagonal contrasts of basal planes observed at the central region of the tubes (Figure 4b) are the Moire fringes produced by the carbon layers sandwiched between the MoS_2 layers and the carbon layers of the inner tube. The average lattice spacing measured from these fringes was on the order of 0.337

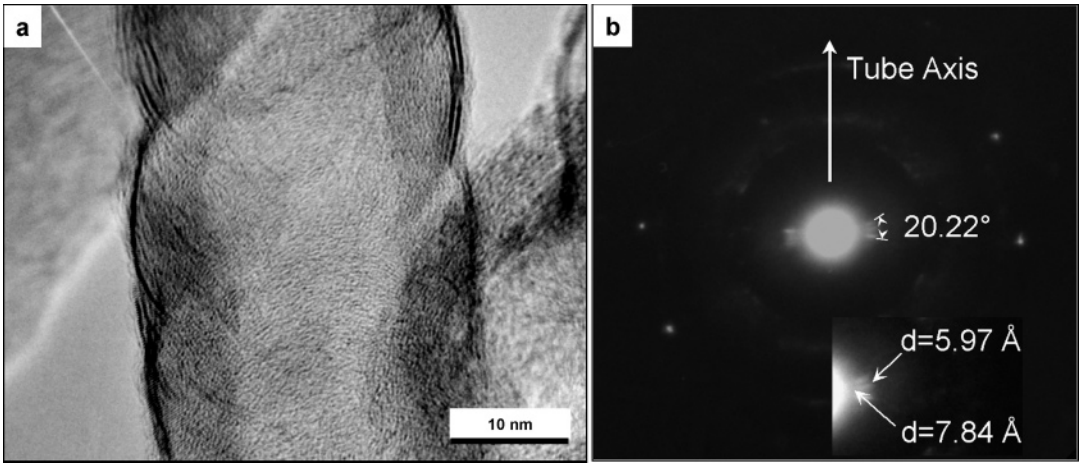

Figure 7. Local analysis of a twisted MoS_2−C nanotube: (a) TEM micrograph and (b) NBEDP obtained at 40 cm of camera length.

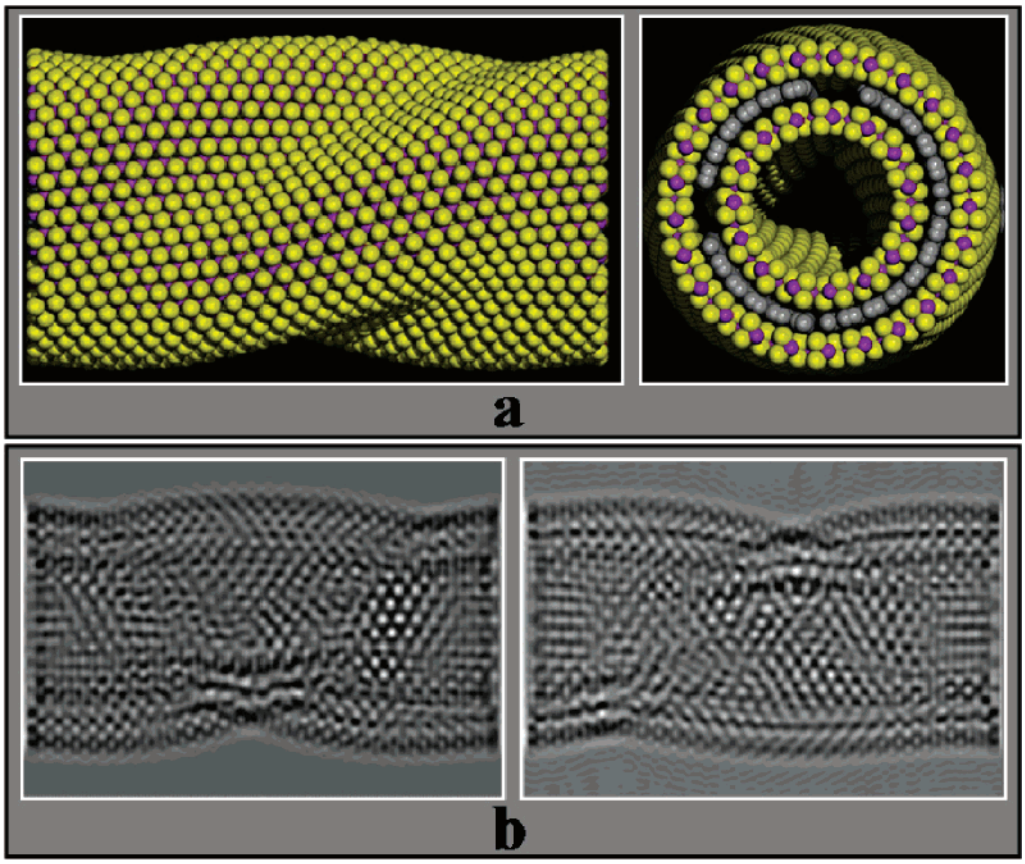

Figure 8. Stable configuration of a carbon-intercalated MoS_2 nanotube produced by sandwiching graphite sheet fragments between the MoS_2 layers: (a) perpendicular and parallel views of the theoretical model and (b) simulated HRTEM images for two different orientations of the model.

nm. This lattice spacing value is due to interference produced by two distinct lattices which has also been observed even in pure MoS_2 nanotubes with a twisted morphology.[10]

The presence of graphite inside the main tube is further verified by recording the EELS spectra of the samples in diffraction mode, which apart from the chemical composition reveal the nature of the chemical bonding of the atoms with their neighbors. The EELS spectrum obtained from a single tube reveals the characteristic peaks of Mo at 35 eV (N-edge) and S at 165 eV (L-edge) and the characteristic profile of graphite carbon at 284 eV (K-edge) (Figure 5). The carbon K-edge profile (Figure 5c) does not present additional fine structure associated with any Mo_xC_y compound. The effect of carbon intercalation with MoS_2 in EELS spectra has been studied by Berhault and co-workers,[37] who additionally found a fine structure in the carbon K-edge profile corresponding to a Mo_2C phase at 295 eV associated with a σ^* state. However, the EELS spectra obtained from our MoS_2−C tubes revealed only the 284 eV (K-edge) peak of carbon graphite without any additional features, indicating the absence of any Mo_xC_y compound formation.

To understand the formation and growth mechanism of these intercalated nanotubes, a sequence of graphite layers intercalated with stoichiometric concentric MoS_2 sheets were simulated by molecular dynamics based on geometry manipulation and optimization.[10] Once the structure was generated, the potential

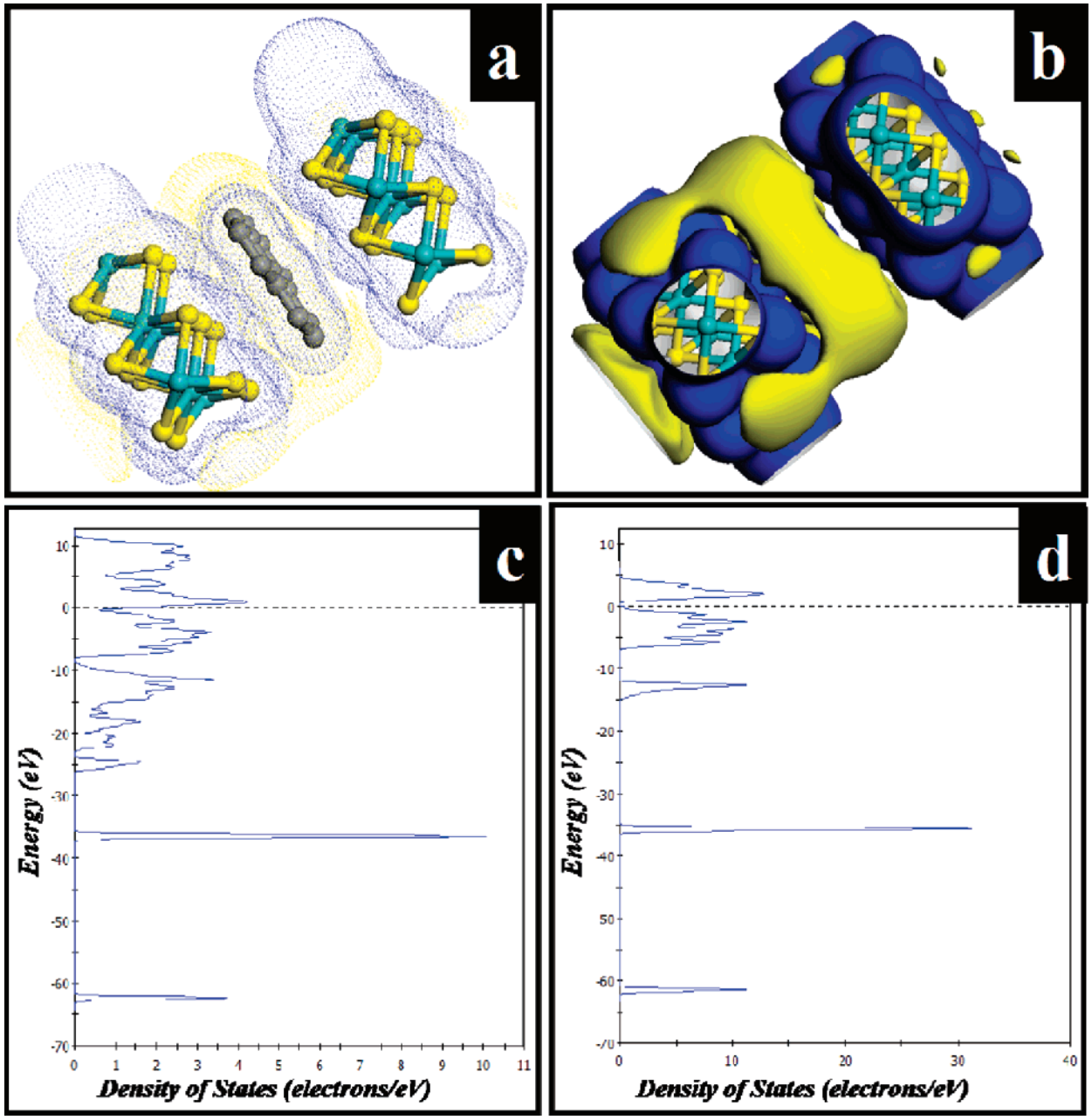

Figure 9. Quantum mechanical analysis of the (a) charge density distribution in MoS_2 + C, (b) electrostatic potential isosurface for MoS_2 + C, (c, d) and DOS spectrum for (c) MoS_2 + C and (d) MoS_2. Green, yellow, and gray balls correspond to Mo, S, and C atoms, while the yellow and blue surfaces correspond to negative and positive polarities, respectively.

energy was minimized using the Cerius[2] molecular simulation software of Accelerys. The coaxial nanotube was then relaxed by Cerius[2] using the Smart Minimizer method and UFF-VALBOND potential. In Figure 6, the optimized simulated structure consisting of a graphite layer between two MoS_2 layers is presented. We can see the distance between two MoS_2 layers is about 7.5 Å, which is very close to the average lattice spacing obtained from our HREM images and nanobeam electron diffraction patterns (NBEDPs) (Figure 7b).

However, our experimentally obtained nanotubes are neither perfect (see Figure 4) nor of homogeneous morphology (see Figure 7a). The local contrast at the nanotube boundaries presented in Figure 7a shows several waistlines with an interlayer distance of about 7.4 Å which corresponds to MoS_2 layers intercalated with carbon. Also a lighter contrast zone inside the main tube that corresponds to the graphite lattice fringes of the coaxial multiwall carbon nanotubes is visible in the figure. The contrast and morphology of the bent walls correspond to the typical twisted hollow cylindrical structure as supported by our electron diffraction results.

NBEDPs of the twisted structures were taken at 40 cm of camera length in a JEOL 2010 microscope. The helical nature of the coaxial MoS_2−C nanotubes is clearly evident in the (0002) reflection (Figure 7b) of the sample. The knob features of the (0002) reflection reveal internal structure with two linear spots symmetric with respect to the equatorial line. The appearance of such split reflections in NBEDPs is well-known for chiral nanotubes. In the present case, the appearance of split reflections in NBEDPs is the consequence of the chiral behavior of our coaxial multiwall nanotubes of the binary irregular phase. As the intercalated graphite did not fill the MoS_2 slabs completely, several mechanical defects were generated in the intercalation process, causing a change in the curvature of the one-dimensional host structure. The appearance of a line

structure in the (0002) reflection in NBEDPs of multishell chiral MoS_2 nanotubes is demonstrated by L. Margulies and co-workers.[38] Nevertheless, in the particular case of a binary multiwall nanotube, the interpretation of the NBEDP is not easy. To index the diffraction pattern, internal and external diameters of each symmetric pair of linear spots along the equatorial reflection are measured. The *d* spacings measured through internal and external diameters were 7.84 ± 0.05 and 5.97 ± 0.05 Å, respectively, while the angle between the linear spots was $20.2 \pm 0.05°$.

To explain the chirality in our MoS_2−C binary nanostructures, several model structures were constructed by introducing graphite sheets into the walls of a MoS_2 nanotube host. We introduced graphite sheets into the layers of a MoS_2 nanotube to induce a mechanical stress in it. Generation of positive and negative curvatures due to induction of topological defects in chiral MoS_2 nanotubes was demonstrated theoretically by Seifert and co-workers[39] recently. On relaxation, our model structures revealed torsions on its one-dimensional configuration. Parallel and perpendicular views of the lowest energy configuration along with a couple of simulated HREM images[30] for a structure formed by introducing a discontinuous graphite sheet between two MoS_2 layers are shown in Figure 8. The configuration is obtained when graphite fragments are internally distributed in the MoS_2 nanotube sheets, generating mechanical stress in the regions where there is no carbon. The contrasts observed in the simulated HREM images are in good agreement with the contrasts obtained in the experimental micrographs (Figure 8b). Particularly, the contrast at the nanotube borders argues well for the experimental observation of varied interlayer distances between (0002) planes in our system.

To explore the possible electronic changes that occurred by the intercalation process in our MoS_2 nanostructures, we performed quantum mechanical calculations for a system consisting of a graphite layer between two MoS_2 layers. The calculated charge density and electrostatic potential distribution for the system are shown in parts a and b, respectively, of Figure 9. In addition, the densities of states (DOS) for MoS_2+C and MoS_2 layered materials are plotted in parts c and d, respectively, of Figure 9. From the charge density and electrostatic potential distributions, it is clear how the presence of the graphite layer generates a high concentration of electrons between the MoS_2 layers. Furthermore, comparing the calculated DOS results for MoS_2+C and MoS_2 (Figure 9c,d), it is possible to observe that while the main features in the DOS spectrum for MoS_2 remained unchanged, the number of electrons in the occupied bands increased drastically on incorporation of the graphite sheet between MoS_2 layers. In fact, the presence the carbon layer between MoS_2 layers changes the perturbation condition and facilitates electrons to move from one MoS_2 layer to the other. Furthermore, the introduction of excess charge into the MoS_2 layers can lead to mechanical deformation as observed in the case of carbon nanotubes.[40]

Our quantum mechanical calculations indicate that some energetically stable structures can be formed by putting graphite fragments between MoS_2 slabs. However, the incorporation of carbon layers causes a drastic change in the electronic properties of MoS_2, which may affect its catalytic properties. A further study is needed to explore the catalytic behavior of this MoS_2−C binary-phase nanostructure.

Conclusions

We could synthesize graphite-incorporated MoS_2 tubular nanostructures. These micrometer long nanostructures consist of alternating carbon and MoS_2 layers at the outer walls and multiwall carbon nanotubes inside. While the van der Waals interlaminar interaction allows the intercalation of carbon with MoS_2 layers, the interlayer spacing of MoS_2 increases due to incorporation of carbon sheets between them. Incorporation of a fragmented carbon sheet inside MoS_2 layers introduces mechanical strain, induces deformation in the linear tubular structure of MoS_2, and originates chiral properties in them. Our theoretical calculations predicted the formation of stable carbon-intercalated MoS_2 tubular structures with a drastic change in their electronic properties which may favor their catalytic and optoelectronic applications. However, a detailed theoretical analysis is needed to explore the possible applications of these materials. The use of MoS_2 nanotubes as a template for the synthesis of new binary-phase tubular structures is demonstrated.

Acknowledgment is due to the CONACYT-Mexico for support of this project through Grant 31199-U. Acknowledgment is also due to PAPIIT-UNAM Research Projects IN108303-3 and IX107204. Special recognition is due to Leticia Carapía-Morales for her exceptional SEM work. Finally, recognition is due to the Physics Institute Central Microscopy Laboratory at UNAM for permitting the use of its TEM facilities.

References and Notes

(1) Iijima, S. *Nature* **1991**, *354*, 56.
(2) Gudiksen, M. S.; Lauhon, L. J.; Wang, J.; Smith, D. C.; Lieber, C. M. *Nature* **2002**, *415* (6872), 617.
(3) Fan, S. S.; Chapline, M. G.; Franklin, N. R.; Tombler, T. W.; Cassell, A. M.; Dai, H. J. *Science* **1999**, *283* (5401), 512.
(4) Tenne, R.; Zettl, A. K. Carbon Nanotubes. *Top. Appl. Phys.* **2001**, *80*, 81.
(5) Nath, M.; Rao, C. N. R.; Popovitz-Biro, R.; Albu-Yaron, A.; Tenne, R. *Chem. Mater.* **2004**, *16* (11), 2238.
(6) Hacohen, Y. R.; Popovitz-Biro, R.; Grunbaum, E.; Prior, Y.; Tenne, R. *Phys. Chem. Chem. Phys.* **2003**, *58*, 1644.
(7) Tenne, R. *Chem.*—Eur. J. **2002**, *8* (23), 5297.
(8) Wilson, M. *Nano Lett.* **2004**, *4* (2), 299.
(9) Minot, E. D.; Yaish, Y.; Sazonova, V.; McEuen, P. L. *Nature* **2004**, *428* (6982), 536.
(10) Santiago, P.; Ascencio, J. A.; Mendoza, D.; Pérez-Alvarez, M.; Espinoza, A.; Reza-San Germán, C.; Schabes-Retchkiman, P.; Camacho-Bragado, G. A.; José-Yacamán, M. *Appl. Phys. A* **2004**, *78*, 513.
(11) Bandyopadhyay, S.; Millar, A. E.; Chang, H. C.; Banerjee, G. F.; Yuzhakov, V.; Yues, D. F.; Ricker, R. E.; Jones, S.; Eastman, J. A.; Baugher, E.; Chandrasekhar, M. *Nanotechnology* **1996**, *7*, 360.
(12) Ozao, R.; Yoshida, H.; Ichimura, Y.; Inada, T.; Ochiai, M. *J. Therm. Anal. Calorim.* **2001**, *64*, 915−922.
(13) Ozao, R.; Ochiai, M.; Yoshida, H.; Ichimura, Y.; Inada, T. *J. Therm. Anal. Calorim.* **2001**, *64*, 923−932.
(14) Ozao, R.; Yoshida, H.; Inada, T. *J. Therm. Anal. Calorim.* **2002**, *69*, 925−931.
(15) Bandyopadhyay, S.; Miller, A. E.; Chang, H. C.; Banerje, G.; Yuzhakov, V.; Yue, D. F.; Ricker, R. E.; Jones, S.; Eastman, J. A.; Baugher, E.; Chandrasekhar, M. *Nanotechnology* **1996**, *7*, 360.
(16) Benavente, E.; Santa Ana, M. A.; Mendizábal, F.; González, G. *Coord. Chem. Rev.* **2002**, *224*, 87.
(17) Ascencio, J. A.; Perez-Alvarez, M.; Molina, L. M.; Santiago, P.; Jose-Yacaman, M. *Surf. Sci.* **2003**, *526* (3), 243.
(18) Hacohen, Y. R.; Popovitz-Biro, R.; Prior, Y.; Gemming, S.; Seifert, G.; Tenne, R. *Phys. Chem. Chem. Phys.* **2003**, *5* (8), 1644.
(19) Mayer, A. *Carbon* **2004**, *42* (10), 2057.
(20) Helveg, S.; Lopez-Cartes, C.; Sehested, J.; Hansen, P. L.; Clausen, B. S.; Rostrup-Nielsen, J. R.; Abild-Pedersen, F.; Norskov, J. K. *Nature* **2004**, *427* (6973), 426.
(21) Grenzer, J.; Zeimer, U.; Grigorian, S. A.; Feranchuk, S.; Pietsch, U.; Fricke, J.; Kissel, H.; Knauer, A.; Weyers, M. *Phys. Rev. B* **2004**, *69* (12), 125316.
(22) Natsuki, T.; Tantrakarn, K.; Endo, M. *Appl. Phys. A: Mater. Sci. Process.* **2004**, *79* (1), 117.
(23) Abe, H.; Shimizu, T.; Ando, A.; Tokumoto, H. *Physica E (Amsterdam)* **2004**, *24* (1−2), 42.
(24) Cerius^2, ver. 3.5, Accelrys, San Diego, CA, 1997.
(25) Maiti, A. *CMES*—Comput. Model. Eng. Sci. **2002**, *3* (5), 589.
(26) Shibutani, Y.; Ogata, S. *Modell. Simul. Mater. Sci. Eng.* **2004**, *12* (4), 599.

(27) Deaton, R.; Kim, J.; Chen, W. J. *Appl. Phys. Lett.* **2003**, *82* (8), 1305.

(28) Zelenski, C.; Dorhout, P. *J. Am. Chem. Soc*. **1998**, *120*, 734.

(29) Gómez, A.; Beltran del Rio, L. SimulaTem Software, http://fisica.unam.mx.

(30) CASTEP software as part of Cerius2 by Accelrys, San Diego, CA, 2000.

(31) Perdew, J. P.; Burke, K.; Ernzerhof, M. *Phys. Rev. Lett*. **1996**, *77*, 3865.

(32) Benavente, E.; Santa Ana, M. A.; Mendizábal, F.; González, G. *Coord. Chem. Rev.* **2002**, *224*, 87.

(33) Zak, A.; Feldman, Y.; Lyakhovitskaya, V.; Leitus, G.; Popovitz-Biro, R.; Wachtel, E.; Cohen, H.; Reich, S.; Tenne, R. *J. Am. Chem. Soc*. **2002**, *124*, 4747.

(34) AnalySIS, Version 3.1.103, Soft Imaging System, Münster, Germany, 1999.

(35) . Sato, K.; Noguchi, M.; Demachi, A.; Oki, N.; Endo, M. *Science* **1994**, *264*, 556.

(36) Camacho-Bragado, G. A.; Santiago, P.; Marin-Almazo, M.; Espinosa, M.; Romero, E. T.; Murgich, J.; Rodríguez Lugo, V.; Lozada-Cassou, M.; Yacaman, M. J. *Carbon* **2002**, *40*, 2761.

(37) Berhault, G.; Mehta, A.; Pavel, A. C.; Yang, J.; Rendon, L.; Yacaman, M. J.; Cota-Araiza, L.; Duarte-Moller, A.; Chianelli, R. R. *J. Catal.* **2001**, *198*, 9.

(38) Margulies, L.; Dluzewski, P.; Feldman, Y.; Tenne, R. *J. Microsc.* **1996**, *181*, 68.

(39) Seifert, G.; Terrones, H.; Terrones, M.; Jungnickel, G.; Frauenheim, T. *Phys. Rev. Lett.* **2000**, *85*, 146.

(40) Baughman, R. H.; Cui, C.; Zakhidov, A. A.; Iqbal, Z.; Barisci, J. N.; Spinks, G. M.; Wallace, G. G.; Mazzoldi, A.; De Rossi, D.; Rinzler, A. G.; Jaschinski, O.; Roth, S.; Kertesz, M. *Science* **1999**, *284*, 1340.